Laser Oscillating Welding of TC31 High-Temperature Titanium Alloy

Zhimin Wang [1], Lulu Sun [2], Wenchao Ke [3], Zhi Zeng [3], Wei Yao [2] and Chunming Wang [4],*

[1] School of Mechanical Science and Engineering, Huazhong University of Science and Technology, Wuhan 430074, China; wangzhimin2020@yeah.net

[2] Special Machining Department, Beijing Hangxing Machine Manufacture Co., Ltd., Beijing 100013, China; sunll@live.cn (L.S.); yaowei239@sina.com (W.Y.)

[3] School of Mechanical and Electrical Engineering, University of Electronic Science and Technology of China, Chengdu 611731, China; ke@std.uestc.edu.cn (W.K.); zhizeng@uestc.edu.cn (Z.Z.)

[4] School of Materials Science and Engineering, Huazhong University of Science and Technology, Wuhan 430074, China

* Correspondence: cmwang@hust.edu.cn; Tel./Fax: +86-027-875-438-94

Abstract: The joining of high-temperature titanium alloy is attracting much attention in aerospace applications. However, the defects are easily formed during laser welding of titanium alloys, which weakens the joint mechanical properties. In this work, laser oscillating welding was applied to join TC31 high-temperature titanium alloy. The weld appearance, microstructure and mechanical properties of the laser welds were investigated. The results show that sound joints were formed by using laser oscillating welding method, and a large amount of martensite was presented in the welds. High mechanical properties were achieved, which was approaching to (or even equaled) the strength of the base material. The joints exhibited a tensile strength of up to 1200 ± 10 MPa at room temperature and 638 ± 6 MPa at 923 K. Laser oscillating welding is beneficial to the repression of porosity for welding high-temperature titanium alloy.

Keywords: laser oscillating welding; high temperature titanium alloy; microstructure; mechanical properties

1. Introduction

Titanium alloys exhibit high specific strength, excellent corrosion resistance and high thermal strength, which have been widely used in aerospace field to reduce weight [1–4]. In recent years, as the flight speed and distance of air vehicles increase significantly, traditional titanium alloys such as TC4, TA15 cannot cover the operating requirements. High-temperature titanium alloys possess excellent mechanical properties at high temperature, and the service temperature of these alloys is increased to above 873 K [5–7]. Due to these excellent performances, high-temperature titanium alloys have become advanced materials in aerospace applications, such as the components of aircraft engines, wings and rudders [8]. TC31 alloy is a high-temperature double-phase titanium alloy of the Ti-Al-Sn-Zr-Mo-Nb-W-Si system with high aluminum content, which can be used in a temperature range of 923–973 K [9–11]. This alloy also has good durability and creep properties under high load and high temperature [12]. Therefore, it has shown a prefect application in the aerospace field. To obtain a sound joint with good mechanical performance is a key factor to achieve structural integrity, light weight and low-cost manufacturing for its applications.

As an important part of laser manufacturing technology, laser welding is currently one of the most notable and most promising welding technologies. Due to its advantages of high quality, low

deformation, high precision, high efficiency and high speed, laser welding technology has become a key joining method for airplanes and automobiles—with improved safety and structural weight reduction, clean and efficient shipbuilding—and nuclear power plant construction [13,14]. It is an effective way to achieve the upgrading of traditional industrial structures and achieve energy saving and emission reduction. Laser welding has been able to achieve the joining of many types of materials, and has many unmatched advantages of fusion welding processes [15–17]. For example, laser welding is used to weld aircraft skin and stringers [18,19]. Compared with riveted structure, the weight and cost of airplane is reduced dramatically. However, due to high degree of alloying and low plasticity-reserve for high-temperature titanium alloy, the possibility of cracking of the joint is higher than that of traditional titanium alloy, and it is easy to generate weld defects during welding [20–22]. The fewer the weld defects, the better the weld mechanical performances. In addition, the mechanical performances have a relationship with the laser welding parameters, such as laser power and welding speed, as verified by finite element method (FEM) and artificial neural network (ANN) simulation techniques [23–25]. Recently, laser oscillating welding has been promising in reducing the weld porosities and increasing the weld ductility [26]. However, most of the studies about laser oscillating welding purely focused on the mechanism of porosity suppression; there is a need for an exhaustive description of the relationship between the weld mechanical performances and the process parameters.

The paper gives the comparison of the weld profiles, microstructures and mechanical properties under different laser powers, welding speeds, laser beam weaving frequencies and amplitudes to obtain the sound welding parameters. In the study, high-temperature titanium alloy TC31 was welded by a laser oscillating welding method. The appearance, internal quality and microstructure of the weld under different welding parameters were observed. The mechanical properties of the joints at room temperature and high temperature were investigated. The mechanism for improved joint strength is also discussed.

2. Experimental

The base metal is high-temperature titanium alloy TC31 in this study, and its composition and mechanical properties are listed in Tables 1 and 2, respectively. TC31 alloy was machined into plates with a dimension of 200 mm × 100 mm × 3 mm. The plates were polished with SiC sandpaper, acid pickled in HF solution and ultrasonically cleaned with acetone and ethyl alcohol.

Table 1. The composition of high-temperature titanium alloy TC31 (wt%).

Element	Ti	Al	Sn	Zr	Mo	Nb	W	Si
Composition	Balance	6.0–7.2	2.5–3.5	2.5–3.5	1.0–3.2	1.0–3.2	0.3–1.2	0.1–0.5

Table 2. Mechanical properties of alloy TC31 with the thickness of 3 mm at room temperature and high temperature 923 K.

Temperature	UTS/MPa	YS/MPa	Elongation/%
RM	1205	1091	15.2
650 °C	648	-	17.3

Butt welding experiments were carried out on the base material using laser oscillating welding method. The laser welding parameters for two welding methods are listed in Table 3. In laser oscillating welding experiments, the laser beam oscillated in a figure-eight manner with the weaving frequency of 200–400 Hz and the weaving amplitude of 0.1–0.5 mm. The laser power was in the range of 1900–2100 W, and the welding speed is in the range of 1200–1800 mm/min. Since titanium alloy is easily reacted with ambient gases, argon was used as shielding gas with the flow rate of 15 L/min during welding process. The laser focused on the workpiece surface with a diameter of

0.45 mm, defocus amount of 0 and a working distance of 247 mm. A D50 wobble seam oscillating head (IPG Laser GmbH, Burbach, Germany) was utilized to adjust the oscillating frequency and amplitude.

Table 3. Laser oscillating welding parameters.

Sample	Weaving Frequency of Laser Beam (Hz)	Weaving Amplitude of Laser Beam (mm)	Laser Power (W)	Welding Speed (mm/min)
W1	200	0.1	1900	1200
W2	200	0.3	2000	1500
W3	200	0.5	2100	1800
W4	300	0.1	2000	1800
W5	300	0.3	2100	1200
W6	300	0.5	1900	1500
W7	400	0.1	2100	1500
W8	400	0.3	1900	1800
W9	400	0.5	2000	1200

After welding, the internal quality of the welds was examined by X-ray nondestructive testing instrument (NDT, MU2000-D) (YXLON International GmbH, Hamburg, Germany) using a tube voltage of 120 kV and a tube current of 3.4 mA. Due to the limitation of capability of equipment, the nondestructive testing was conducted twice on different parts for each sample. The microstructure of the weld was studied by a GX53 metallurgical microscope (Olympus Corporation, Tokyo, Japan) after being etched with Kroll's reagent: 2 mL HF, 6 mL HNO_3 and 92 mL H_2O. X-ray diffraction (XRD, D/MAX-2500) (Rigaku Corporation, Tokyo, Japan) using Cu-K$_\alpha$ radiation was employed to examine the structure of the welds. For X-ray diffraction measurements, a diffractometer with the X-ray tube operating at 40 kV and 200 mA target current was used. The microstructure of the joints was also studied using an electron probe microanalyzer (EPMA, JXA-8100) (JEOL Ltd., Tokyo, Japan). To determine the mechanical properties of the joints at room temperature and high temperature 923 K, the weld plate samples were machined into joint samples with dimensions depicted in Figure 1 for measurement (as GB/T 228.1-2010 standard and GB/T 228.2-2015 standard). The samples were cut along the direction perpendicular to the weld. Tensile tests were performed, respectively, on three joint samples by using a universal testing machine at a tensile speed of 0.5 mm/min. After the tensile test, fracture surfaces of the weld joints were observed by a scanning electron microscope (SEM, JSM-7001F) (JEOL Ltd., Tokyo, Japan) with an energy dispersive spectrometer (EDS, Pegasus XM2 EDS) (EDAX Inc., Mahwah, NJ, USA) system.
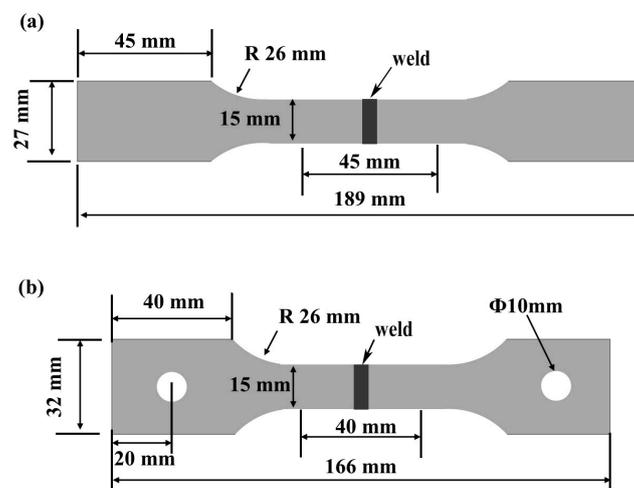

Figure 1. Dimensions of the specimens in tensile testing: (**a**) sample design for room temperature testing; (**b**) sample design for high temperature testing.

3. Results and Discussion

3.1. Weld Appearance and Internal Quality

High-temperature titanium alloy TC31 plate samples were weld under different laser welding conditions listed in Table 3. The front and back appearances of the butt weld joints are shown in Figure 2. As shown in Figure 2, the welds are continuous in the surfaces without cracks, and uniform fish-scale patterns are observed. The samples except samples W5 and W9 display the front appearance as yellow or silvery white. With increasing the laser power up to 2100 W or decreasing welding speed to 1200 mm/min, the front appearances of the welds present a color of green, purple or blue, which indicates that the oxidation of the front appearances is further deepened [27]. By contrast, the back appearance of all the welds is silvery-white in color, indicating an effective protection for the joints through gas shielding. Besides, as can be seen from Figure 2e,i, the back weld width of W5 and W9 samples are obviously larger than those of other samples, indicating the higher heat input.
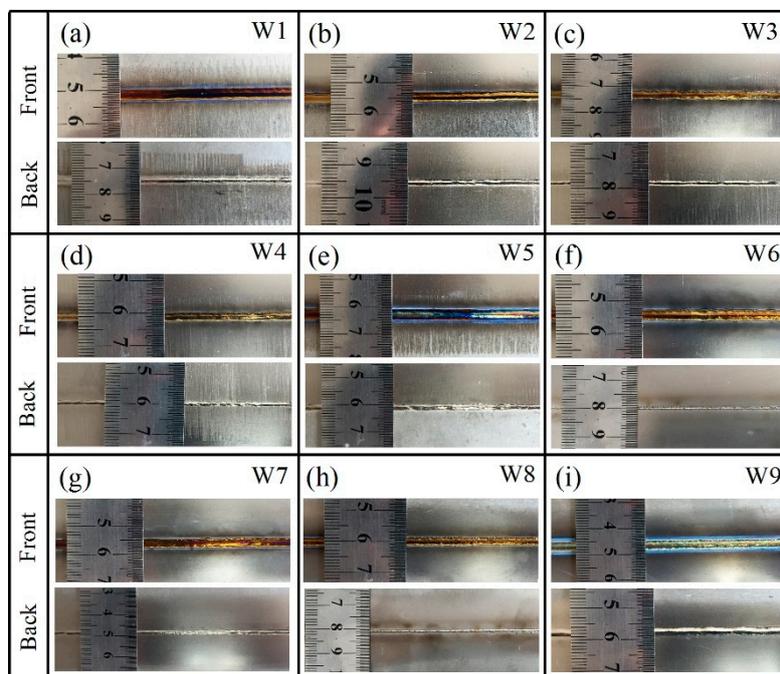

Figure 2. The front and back appearances of the laser-welded TC31 joints: (**a–i**) represent W1 to W9 samples.

For further investigating the internal quality of the welds, the X-ray non-destructive testing was conducted and the result is shown in Figure 3. Except that porosity defects are observed in W8, other joints exhibit sound bonding without lack of fusion, slag or hot cracks.
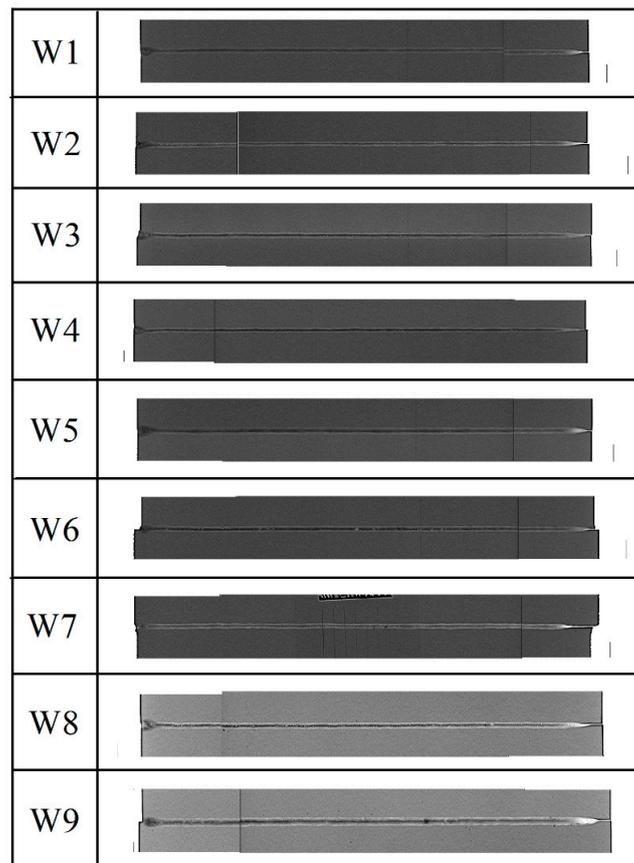
Figure 3. Images of the laser-welded TC31 joints in X-ray detection.

3.2. Microstructure Characterization

Figure 4 shows the optical micrographs of the cross-sections of W1 to W9 laser welded joints. The joints exhibit slight defect of undercut. The undercut with a maximum depth (≈0.165 mm) was occurred in W9 sample, and the undercut imperfection is 0.055t (t is the thickness of the alloy plate), which is lower than the limit of for quality C level (0.1t) according to ISO 5817 standard. Thus, the laser-welded TC31 joints reach the weld quality C level (medium quality requirements). In addition, no misalignment defect was observed in these joints. Three distinct regions in the joints can be observed, i.e., the fusion zone (FZ), the heat-affect zone (HAZ) and the base material (BM). The FZ mainly consists of coarse prior β columnar grains. There are a few equiaxed grains at the junction of the FZ and the HAZ. The columnar grains in the middle of cross section grow horizontally and towards the weld centerline, while the columnar grains closed to the weld front and back surfaces grow from the weld fusion line to the weld surface. Figure 5 shows the magnification view of the fusion zone and heat-affected zone of the W5 joint. It can be seen that there is a large amount of staggered needle-shaped α' phases inside the columnar crystal, which is the typical structure of martensite [28].

The phases in the FZ of the welded joints are examined by XRD. The examination is carried out on W2. As shown in Figure 6, the XRD pattern consists of the peaks corresponding to α'-Ti phase, and no peak corresponding to β-Ti phase is observed. This result implies that the major phase in the weld is α'-Ti phase. For further analyzing the microstructure of the joints, EPMA analysis is also conducted on the weld of W2. The backscattered electron image of the cross-section of the joint is shown in Figure 7. It is seen that the laser welded joint is free from obvious defects, such as voids and cracks. The BM consists of elongated α grain and intergranular β grain (Figure 7a). A large amount of acicular Ti and columnar prior β grain boundaries can be observed in the FZ as shown in Figure 7b,c, which implies that the prior β phase gradually transform into the secondary α phase [1,29].
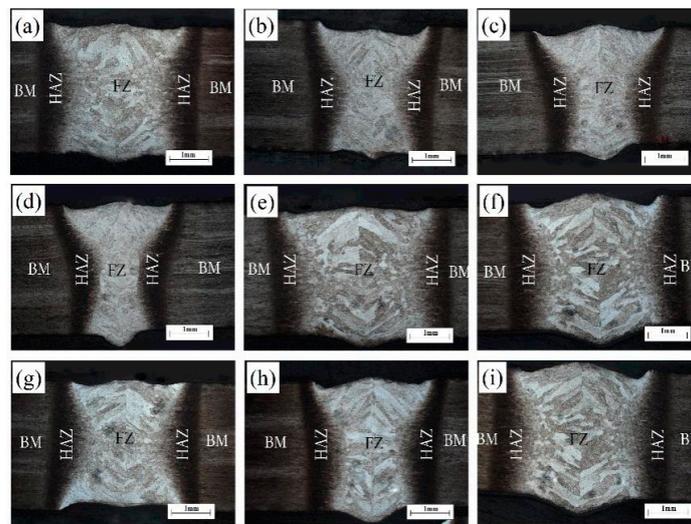
Figure 4. Optical micrographs of cross sections of as the laser-welded TC31 joints: (**a**–**i**) represent W1 to W9 samples.
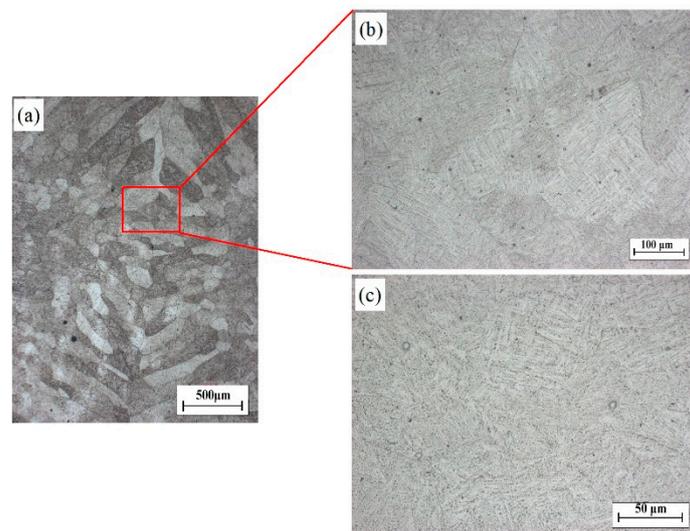

Figure 5. Magnification view of fusion zone and heat-affected zone of W5 joint: (**a**) fusion zone and heat-affected zone; (**b**) high-magnification scanning electron microscope image of the rectangular region in (**a**); (**c**) high-magnification scanning electron microscope image of (**b**).
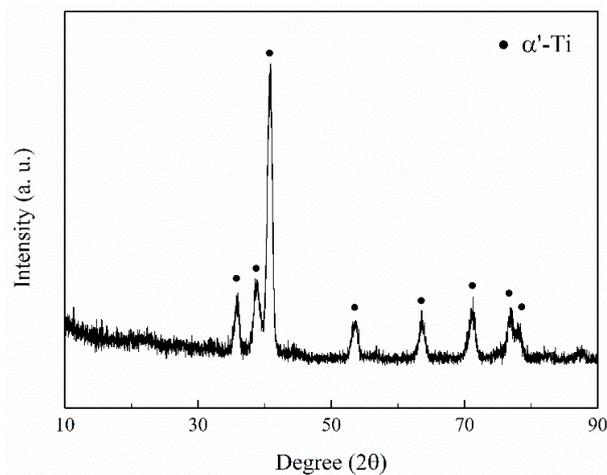

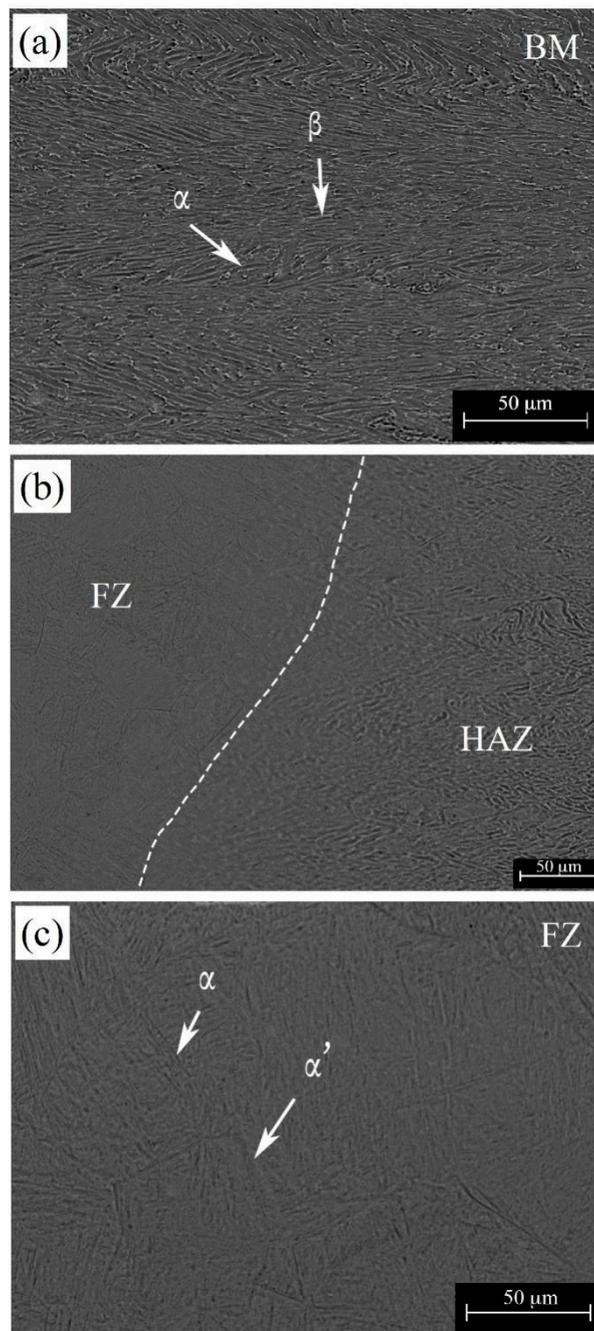**Figure 6.** X-ray diffraction pattern of W2 weld.

Figure 7. Backscattered electron images of the cross-section of W2 joint: (**a**) Base material (BM); (**b**) Heat-affect zone/Fusion zone (HAZ/FZ) transition zone; (**c**) Fusion zone (FZ).

The formation mechanism of the joint is discussed as follows. The microstructural transformation of the welds for TC31 laser-welded joints are influenced by the welding thermal cycle and the ingredient distribution of the bonding zone [13]. As illustrated in Figure 4, the size of prior grain boundaries significantly increased. This may be due to the growth of grain is sensitive to overheating. During the laser welding process, the unmelt BM closed to the bottom of welding pool and the top of heat-affecting zone is under the condition of ultra-high temperature reaching or exceeding the liquidus temperature of phase. The grain nucleates at the surface of partially molten base material, and then grow quickly towards the center of the weld. With the growth of columnar grain, the temperature gradient of the melt gradually flattens, and the solute concentration in melt increases, resulting in the constitutional undercooling in the front of the solid-liquid interface increasing and the equiaxed crystals forming

in the center of the weld. Due to the solidification behavior of weld center occur during the final stage of solidification, the growth of the equiaxed crystals is limited by the solidified columnar grains. Moreover, the columnar grains have an insulating effect on the equiaxed grains, which results in the coarse grains in the weld center. Near the surface of the weld, due to the change in heat dissipation conditions in the middle solidification of the weld, the columnar crystal grows toward the surface of the weld, and there is a large angle between the growth direction and the growth direction of the central columnar crystal. Laser welding is a rapid heating and cooling process, rapid quenching will cause martensite transformation of titanium alloy [1]. During the cooling process, the initial β columnar crystals of the weld metal generate α′ phase via shear transformation. It is due to the rapid cooling rate frustrating the atomic diffusion of the β phase. The α′ martensite grows and form one or several primary needle-like martensite parallel to each other, and then form a series of relatively fine secondary needle-like martensite. These secondary martensitic grains stop growing when encountering grain boundary or primary martensite, resulting in the formation of a typical staggered needle-like structure in the welding seam of the laser oscillating welds [29,30].

3.3. Mechanical Properties

The tensile strength of the welded specimens at room temperature are listed in Figure 8, and the photographs of W1 and W2 joints after the tensile test are shown in the insets of Figure 8. It is observed that the average tensile strength of W2 reaches 1200 ± 10 MPa, which is equal to the tensile strength of TC31 alloy. Meanwhile, the average tensile strength of W1, W6, W7 and W9 samples also exhibit high tensile strength, reaching 1183 ± 4 MPa, 1185 ± 31 MPa, 1184 ± 63 MPa and 1190 ± 1 MPa, respectively. The fracture of two specimens of W1 joint occurred at the base material, while the ruptures of W2 specimens occurred in the HAZ. As seen in Figure 8, the W8 sample exhibits relatively low mechanical properties, which is caused by the porosity defects in the weld [31,32].
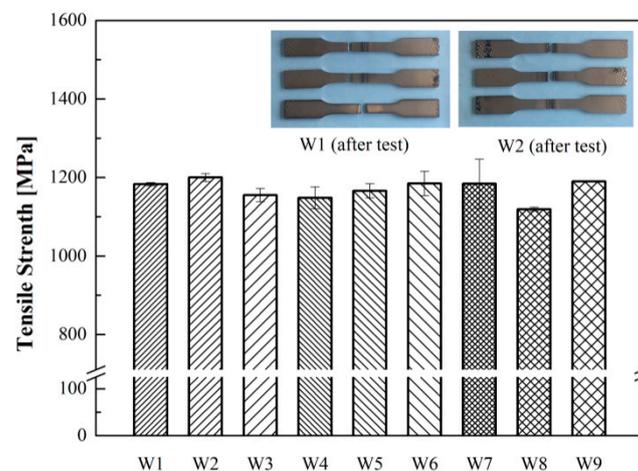

Figure 8. Tensile strength of welded TC31 specimens by wave laser oscillating welding method at room temperature. (The insets show the photographs of W1 and W2 joints after the tensile test.).

Given that the working temperature of TC31 alloy can reach from 923 K to 973 K, the mechanical properties of the joints at high temperature conditions is also essential. The tensile strength of the welded specimens at 923 K are also tested and listed in Figure 9. As seen in Figure 9, the tensile strength of W2 joint reaches 635 ± 3 MPa. Moreover, the highest tensile strength for TC31 specimens by laser oscillating welding at 923K can reach up to 638 ± 6 MPa for W1 joint. The fracture of W1 joint specimens at 923 K occurred at the BM away from the weld seams.
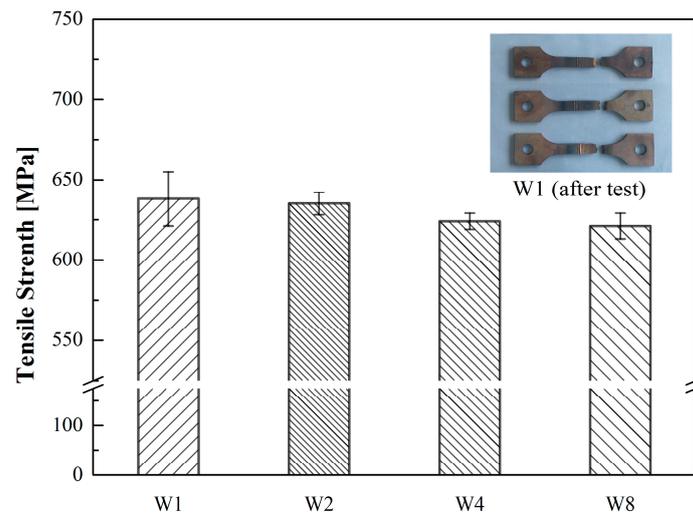
Figure 9. Tensile strength of welded TC31 specimens by laser oscillating welding method at 923 K. (The inset show the photograph of the W1 joint after the high-temperature tensile test.).

In order to investigate the mechanism for the high strength of the joints by laser oscillating welding, the fracture surfaces of the welded joints were examined by SEM. Figure 10 presents the magnified view of the fracture surface of W2 after the tensile test performed at room temperature. A large number of dimples densely distribute on the fracture zone, which is a typical feature of ductile failure. The formation of the dimples implies plastic deformation in the micro regions, which is suggested to be favorable for improving mechanical properties of the joint. Figure 11 presents the magnified view of the fracture surface of W1 joint after the tensile test performed at 923 K. It can be seen from Figure 11 that the area where the fracture is close to the surface of the weld (Figure 11b) and the middle part of the welded joint (Figure 11c,d) show distinct features. Region i fracture morphology shows the characteristics of tough dimple fractures. The fracture surface is rock sugar-like. There are a large number of small dimples on the grain boundaries of the fracture surface and show slip characteristics. This results from nucleus, growth, and connection. Meanwhile, there are also a small number of dimples concentrated in some areas (red dotted area in Figure 11b). As can be seen from Figure 11c,d, there are a large number of dimple structures in Region ii in the middle part of the welded joint. The above results indicate that the joint undergoes ductile fracture under high temperature conditions.

The TC31 joint fabricated by the laser oscillating welding method exhibits high tensile mechanical properties at room temperature, which is exceeding or approaching the mechanical properties of the base alloy. On the one hand, as can be seen from Figures 4 and 7, no defects, such as cracks, inclusions, or unwelded joints, are generated except W8 sample. Laser welding is a rapid melting and solidification process, and it is difficult for the pores formed in the molten pool to escape, which becomes the stress concentration point of the joint. Compared with pulsed laser welding method [12], the content of pores in the weld seam obtained by wave laser oscillating welding is significantly reduced, and the depth-to-width ratio of the weld seam is relatively small. This is due to the adoption of wave laser oscillating welding method, the reciprocating swing of the laser beam on the weld seam causes part of the weld to remelt repeatedly, prolonging the residence time of the molten metal in the weld pool. The deflection of the laser beam also increases the heat input per unit area, reduce the depth-to-width ratio of the weld, which is favorable for the escape of bubbles. Besides, the oscillation of the laser beam causes the air holes to oscillate, which can also provide the stirring force for the welding molten pool, increase the convection and stirring of the molten pool and then eliminate the air holes. This is a favorable factor for improving the mechanical properties of the joint [33–35].
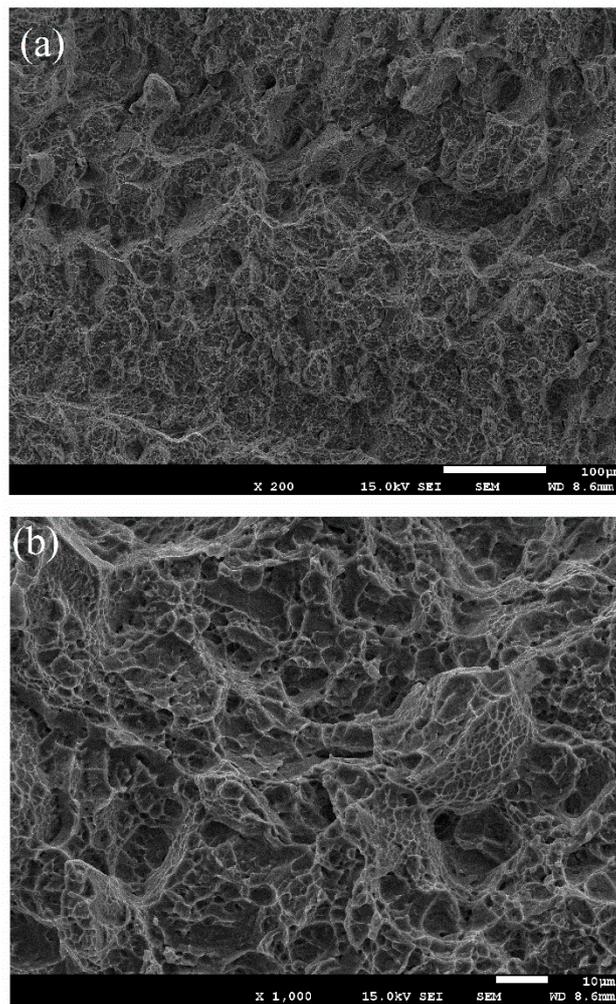
Figure 10. Fracture surface of W2 welded joint after tensile test performed at room temperature, (**b**) is the magnified view of (**a**).
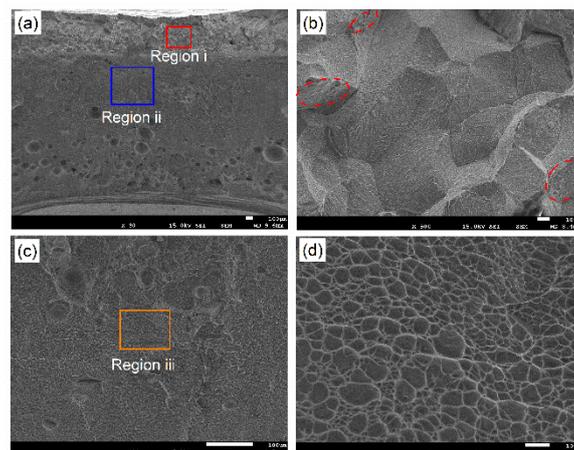

Figure 11. Fracture surface of W1 welded joint after tensile test performed at 923 K: (**a**) macroscopic appearance of fracture; (**b**) high magnification magnification of Region i; (**c**) high magnification magnification of Region ii; (**d**) high magnification magnification of Region iii.

On the other hand, the TC31 high temperature titanium alloy forms a martensite structure in the weld after laser welding. Martensite α' is a supersaturated solid solution of alloying elements in α phase. During the cooling of the weld from the β-phase region to room temperature at a rapid cooling rate,

the atoms have no time to diffuse, and only a small needle-shaped and unevenly distributed martensite structure can be precipitated by shearing. α′ grows inside the initial β columnar crystals, forming one or several parallel primary α′ firstly, and extending through the entire grain over a long distance, stopping at the grain boundary. Then a series of relatively fine secondary needles α′ are formed, which stops at the grain boundaries or primary martensite, resulting in the formation of a typical basket structure in the weld. This structure has good comprehensive properties, such as plasticity, creep resistance and high-temperature endurance strength [1].

4. Conclusions

In this study, high-temperature titanium alloy TC31 was joined by the laser oscillating welding method and good mechanical properties were achieved. The appearance, microstructure and mechanical properties of the welded joints were investigated. High-temperature titanium alloy TC31 formed sound joints by the laser oscillating welding method under the optimized process parameters with the weaving frequency of 200 Hz, weaving amplitude of 0.3 mm, laser power of 2000 W and welding speed of 1500 mm/min. The joints exhibit sound bonding without lack of fusion, slag or hot cracks. The welded region was composed of acicular α′ phase resulting from the high degree of supercooling during the laser welding process. The welded joints exhibit the highest tensile strength of 1200 ± 10 MPa at room temperature, which is approaching that of the base metal. The tensile strength of the joints at the high temperature of 923 K reaches 638 ± 6 MPa. The welded joints exhibit ductile fracture with dimples at both room temperature and high temperature. Considering the mechanical properties of TC31 laser-weld joints at different temperatures and the potential usage environment of this high-temperature titanium alloy, W1 joint with 200 Hz weaving frequency, 0.1 mm weaving amplitude, 1900 W laser power and 1200 mm/min welding speed, exhibit outstanding mechanical properties in this study. Furthermore, laser oscillating welding is beneficial to the repression of porosity for welding high temperature titanium alloy.

Conflicts of Interest: The authors declare no conflict of interest.

References

1. Leyens, C.; Peters, M. *Titanium and Titanium Alloys*; Wiley-VCH: Weinheim, Germany, 2003.
2. Boyer, R.R.; Briggs, R.D. The use of β titanium alloys in the aerospace industry. *J. Mater. Eng. Perform.* **2005**, *14*, 681–685. [CrossRef]
3. Qiao, Y.; Xu, D.; Wang, S.; Ma, Y.; Chen, J.; Wang, Y.; Zhou, H. Corrosion and tensile behaviors of Ti-4Al-2V-1Mo-1Fe and Ti-6Al-4V titanium alloys. *Metals* **2019**, *9*, 1213. [CrossRef]
4. Singh, P.; Pungotra, H.; Kalsi, N.S. On the characteristics of titanium alloys for the aircraft applications. *Mater. Today Proc.* **2017**, *4*, 8971–8982. [CrossRef]
5. Gogia, A.K. High-temperature titanium alloys. *Def. Sci. J.* **2005**, *55*, 149–173. [CrossRef]
6. Evans, R.W.; Hull, R.J.; Wilshire, B. The effects of alpha-case formation on the creep fracture properties of the high-temperature titanium alloy IMI834. *J. Mater. Process. Technol.* **1996**, *56*, 492–501. [CrossRef]
7. Narayana, P.L.; Kim, S.W.; Hong, J.K.; Reddy, N.S.; Yeom, J.T. Tensile properties of a newly developed high-temperature titanium alloy at room temperature and 650 °C. *Mat. Sci. Eng. A* **2018**, *718*, 287–291. [CrossRef]
8. Zhao, Z.L.; Li, H.; Fu, M.W.; Guo, H.Z.; Yao, Z.K. Effect of the initial microstructure on the deformation behavior of Ti60 titanium alloy at high temperature processing. *J. Alloy Compd.* **2014**, *617*, 525–533. [CrossRef]
9. Su, Y.; Kong, F.T.; You, F.H.; Wang, X.P.; Chen, Y.Y. The high-temperature deformation behavior of a novel near-α titanium alloy and hot-forging based on the processing map. *Vacuum* **2019**, *173*, 109135. [CrossRef]

10. Song, X.Y.; Zhang, W.J.; Ma, T.; Ye, W.J.; Hui, S.X. Effect of heat treatment on the microstructure evolution of Ti-6Al-3Sn-3Zr-3Mo-3Nb-1W-0.2Si titanium alloy. *Mater. Sci. Forum* **2016**, *879*, 1828–1833. [CrossRef]

11. Zhang, W.J.; Song, X.Y.; Hui, S.X.; Ye, W.J.; Wang, Y.L.; Wang, W.Q. Tensile behavior at 700 °C in Ti–Al–Sn–Zr–Mo–Nb–W–Si alloy with a bi-modal microstructure. *Mat. Sci. Eng. A* **2014**, *595*, 159–164. [CrossRef]

12. Wu, D.; Wu, Y.; Chen, M.; Xie, L.; Wang, B. High Temperature Flow Behavior and Microstructure Evolution of TC31 Titanium Alloy Sheets. *Rare Met. Mater. Eng.* **2019**, *48*, 3901–3910.

13. Hong, K.M.; Shin, Y.C. Prospects of laser welding technology in the automotive industry: A review. *J. Mater. Process. Technol.* **2017**, *245*, 46–69. [CrossRef]

14. Lopes, J.G.; Oliveira, J.P. A short review on welding and joining of high entropy alloys. *Metals* **2020**, *10*, 212. [CrossRef]

15. Meijer, J. Laser beam machining (LBM), state of the art and new opportunities. *J. Mater. Process. Technol.* **2004**, *149*, 2–17. [CrossRef]

16. Mehrpouya, M.; Gisario, A.; Elahinia, M. Laser welding of NiTi shape memory alloy: A review. *J. Mater. Process. Technol.* **2018**, *31*, 162–186. [CrossRef]

17. Cao, X.; Jahazi, M.; Immarigeon, J.P.; Wallace, W. A review of laser welding techniques for magnesium alloys. *J. Mater. Process. Technol.* **2006**, *171*, 188–204. [CrossRef]

18. Grbović, A.; Sedmak, A.; Kastratović, G.; Petrašinović, D.; Vidanović, N.; Sghayer, A. Effect of laser beam welded reinforcement on integral skin panel fatigue life. *Eng. Fail. Anal.* **2019**, *101*, 383–393. [CrossRef]

19. Reitemeyer, D.; Schultz, V.; Syassen, F.; Seefeld, T.; Vollertsen, F. Laser welding of large scale stainless steel aircraft structures. *Phys. Procedia* **2013**, *41*, 106–111. [CrossRef]

20. Nakai, M.; Niinomi, M.; Akahori, T.; Hayashi, K.; Itsumi, Y.; Murakami, S.; Oyama, H. Microstructural factors determining mechanical properties of laser-welded Ti–4.5Al–2.5Cr–1.2Fe–0.1C alloy for use in next-generation aircraft. *Mat. Sci. Eng. A* **2012**, *550*, 55–65. [CrossRef]

21. Gursel, A. Crack risk in Nd: YAG laser welding of Ti-6Al-4V alloy. *Mater. Lett.* **2017**, *197*, 233–235. [CrossRef]

22. Quazi, M.M.; Ishak, M.; Fazal, M.A.; Arslan, A.; Rubaiee, S.; Qaban, A.; Manladan, S.M. Current research and development status of dissimilar materials laser welding of titanium and its alloys. *Opt. Laser Technol.* **2020**, *126*, 106090. [CrossRef]

23. Casalino, G.; Losacco, A.M.; Arnesano, A.; Facchini, F.; Pierangeli, M.; Bonserio, C. Statistical analysis and modelling of an Yb: KGW femtosecond laser micro-drilling process. *Procedia CIRP* **2017**, *62*, 275–280. [CrossRef]

24. Su, X.; Tao, W.; Chen, Y.B.; Fu, J.Y. Microstructure and tensile property of the joint of laser-MIG hybrid welded thick-section TC4 alloy. *Metals* **2018**, *8*, 1002. [CrossRef]

25. Casalino, G.; Facchini, F.; Mortello, M.; Mummolo, G. ANN modelling to optimize manufacturing processes: The case of laser welding. *IFAC-PapersOnLine* **2016**, *49*, 378–383. [CrossRef]

26. Wang, L.; Gao, M.; Zhang, C.; Zeng, X.Y. Effect of beam oscillating pattern on weld characterization of laser welding of AA6061-T6 aluminum alloy. *Mater. Des.* **2016**, *108*, 707–717. [CrossRef]

27. Li, X.; Xie, J.; Zhou, Y. Effects of oxygen contamination in the argon shielding gas in laser welding of commercially pure titanium thin sheet. *J. Mater. Sci.* **2005**, *40*, 3437–3443. [CrossRef]

28. Zhang, H.; Hu, S.S.; Shen, J.Q.; Li, D.L.; Bu, X.Z. Effect of laser beam offset on microstructure and mechanical properties of pulsed laser welded BTi-6431S/TA15 dissimilar titanium alloys. *Opt. Laser Technol.* **2015**, *74*, 158–166. [CrossRef]

29. Zeng, Z.; Oliveira, J.P.; Bu, X.; Yang, M.; Li, R.; Wang, Z. Laser Welding of BTi-6431S High Temperature Titanium Alloy. *Metals* **2017**, *7*, 504. [CrossRef]

30. Junaid, M.; Baig, M.N.; Shamir, M.; Khan, F.N.; Rehman, K.; Haider, J. A comparative study of pulsed laser and pulsed TIG welding of Ti-5Al-2.5Sn titanium alloy sheet. *Mater. Process. Technol.* **2016**, *242*, 24–38. [CrossRef]

31. Martínez, C.; Guerra, C.; Silva, D.; Cubillos, M.; Briones, F.; Muñoz, L.; Sancy, M. Effect of porosity on mechanical and electrochemical properties of Ti–6Al–4V alloy. *Electrochim. Acta* **2020**, *338*, 135858. [CrossRef]

32. Zhang, W.F.; Liu, X.P.; Wang, H.X.; Dai, W.; Fu, G.C. Quantitative analysis of weld-pore size and depth and effect on fatigue life of Ti-6Al-2Zr-1Mo-1V alloy weldments. *Metals* **2017**, *7*, 417. [CrossRef]

33. Zhao, L.; Zhang, X.D.; Chen, W.Z.; Bao, G. Repression of porosity with beam weaving laser welding. *Trans. China Weld. Inst.* **2004**, *251*, 29–32.

34. Panwisawas, C.; Perumal, B.; Mark Ward, R.; Turner, N.; Turner, R.P.; Brooks, J.W.; Basoalto, H.C. Keyhole formation and thermal fluid flow-induced porosity during laser fusion welding in titanium alloys: Experimental and modelling. *Acta Mater.* **2017**, *126*, 251–263. [CrossRef]

35. Assuncao, E.; Williams, S. Comparison of continuous wave and pulsed wave laser welding effects. *Opt. Laser Eng.* **2013**, *51*, 674–680. [CrossRef]